Elucidating the cellular response of silver nanoparticles as a potential combinatorial agent for cisplatin chemotherapy

Renata Rank Miranda[a,1], Micaella Pereira da Fonseca[a], Barbara Korzeniowska[a], Lilian Skytte[b], Kaare Lund Rasmussen[b] and Frank Kjeldsen[a,1]

[a]*Department of Biochemistry and Molecular Biology, University of Southern Denmark, DK-5230, Odense, Denmark*

[b]*Department of Physics, Chemistry and Pharmacy, University of Southern Denmark, DK-5230, Odense, Denmark*

[1] * Correspondence to:

Renata Rank Miranda

email: renatam.bio@gmail.com

Frank Kjeldsen

email: frankk@bmb.sdu.dk

Abstract

Background: Combination chemotherapy uses drugs that target different cancer hallmarks, resulting in synergistic or additive toxicity. This strategy enhances therapeutic efficacy as well as minimizes drug resistance and side effects. In this study, we investigated whether silver nanoparticles act as a combinatorial partner to cisplatin. In so doing, we compared post-treatment biological endpoints, intracellular drug accumulation, and changes in the proteome profile of tumoral and normal cell lines.

Results: Combinatorial treatment corresponded to cytotoxicity and oxidative stress in both cell lines, yet was substantially more effective against tumoral cells. Proteome analysis revealed that proteins related to energy metabolism pathways were upregulated in both cell lines, suggesting that combinatorial treatment corresponded to energetic modulation. However, proteins and upstream regulators involved in the cell cycle were downregulated, indicating reduced cell proliferation. The response to oxidative stress was markedly different in both cell lines; downregulation of antioxidant proteins in tumoral cells, yet upregulation of the antioxidant defense system in normal cells. These outcomes may have prevented further cell damage and avoided higher cell death rates in normal cells.

Conclusions: Taken together, our results indicate that combining silver nanoparticles with cisplatin increases the therapeutic efficacy of the latter, and the combination warrants further exploration for future therapies.

Keywords: silver nanoparticles, combination chemotherapy, proteomics, cell viability, metal uptake

Background

Nanotechnology arises from unique properties that are attributable to nanoscale structure, and has substantial transformative potential (1,2). Disciplines such as physics, chemistry, biology and medicine make use of these properties. In biomedicine, particularly cancer therapy, nano-sized materials have helped researchers improve existing treatments, and devise new treatments (e.g., pharmaceutical nanocarriers, photothermal therapy, and gene therapy) and diagnostics (e.g., nanosensors and bioimaging agents) (3–6).

Silver nanoparticles (AgNPs) are particularly interesting for cancer therapy due to their potential antitumoral effect, demonstrated by many *in vitro* studies. It has been shown that AgNPs may hinder cancer cell homeostasis by triggering an increase in reactive oxygen species (ROS), which corresponds to decreased proliferation rates as well as macromolecular damage and cell death (7–10). Moreover, AgNPs may also disrupt important cancer hallmarks, such as glucose metabolism and drug resistance. Exposure to AgNPs corresponds to decreased lactate production and downregulation of glycolytic enzymes (11,12), and inhibited efflux activity of multidrug resistance transporters in cancer cells (13,14). Researchers have also observed antitumoral effects of AgNPs in solid tumors of animal models, leading to inhibition of lymphosarcoma progression in rats (15), reduced tumor volume in Dalton's ascites tumors in mice (16), and efficacy against triple-negative breast cancer xenografts in mice (17).

Taken together, these findings underscore the potential of AgNPs as an attractive candidate for the design of antitumoral drugs and treatments. We hypothesize that AgNP toxicity might be useful for enhancing traditional chemotherapy, by synergetic toxicity. In this study, we used AgNPs as a combinatorial agent for cisplatin (CDDP), a widely used antineoplastic drug for several cancers. We conducted mass spectrometry (MS)-

based proteomics analyses to reveal molecular events triggered by combined AgNPs/CDDP exposure in a hepatocarcinoma cell line (HepG2) and a normal hepatocyte cell line (THLE2). We also investigated changes in biological endpoints (e.g., levels of viability and ROS) and intracellular metal content after treatment in both cell lines. Our AgNPs/CDDP combination was toxic to both cell lines. However, the treatment was substantially more effective against tumoral cells and therefore warrants further exploration for cancer therapies.

Methods

Characterization of AgNPs

We obtained spherical AgNPs (10-nm diameter, in citrate buffer: 1 mg/mL, 2 mM) from Nanocomposix. We characterized the nanoparticles' size distribution by DLS and zeta potential (Zetasizer Nano ZS, Malvern Instruments, US). Particle shape analysis, kindly provided by Nanocomposix, was accessed with electron transmission microscope (JEOL 1010, Tokyo, Japan).

Culture of normal and tumoral liver cell lines

We cultured HepG2 cells (Sigma–Aldrich) as a monolayer in high-glucose Dulbecco's modified Eagle's medium (DMEM) supplemented with 10% v/v inactivated fetal bovine serum (FBS) and antibiotics (10 U/mL penicillin and 10 µg/mL streptomycin), at 37°C and 5% CO_2. Cells at passages 112–120 were utilized to conduct the experiments. We plated normal human liver cell line THLE2 (ATCC) on culture flasks pre-coated with a solution containing 0.01 mg/mL fibronectin, 0.03 mg/mL bovine collagen type I, and 0.01 mg/mL bovine serum albumin dissolved in DMEM medium. These cells were cultured as a monolayer in bronchial epithelium basal medium (Lonza),

supplemented with bronchial epithelial growth medium (Lonza) and 10% v/v FBS, at 37°C and 5% CO_2. We used cells at passages 3–6 to conduct the experiments.

Treatment protocol

We seeded cells onto a 96-well microplate for biochemical analyses, a six-well plate for metal quantification, and 100-mm petri dishes for proteomics analyses. The seeding density applied for HepG2 and THLE2 cells was 1×10^5 and 2×10^4 cell/mL, respectively.

After 24 h, we replaced the medium with fresh complete medium containing AgNPs, CDDP, or a combination of both. We treated cells for 24 h using appropriate controls.

Cell viability assay

At the end of the treatment period, we investigated 3-(4,5-dimethylthiazol-2-yl)-2,5-diphenyltetrazolium bromide (MTT, Sigma-Aldrich) metabolism in both cell lines after incubating the cells with 0.5 mg/L MTT for 2 h. Subsequently, cells were washed with phosphate-buffered saline (PBS), and formazan was solubilized with 100 µL dimethyl sulfoxide. For the assay, we measured the absorbance at 560 nm using a FLUOstar Omega plate reader (Germany).

ROS levels

We evaluated cytosolic H_2O_2 levels with 2',7'-dichlorodihydrofluorescein diacetate (H_2DCF-DA, Sigma-Aldrich) and mitochondrial superoxide levels with MitoSOX Red (Thermo Fisher). After exposure, cells were incubated with either 10 µM H_2DCF-DA or 5 µM MitoSOX in fresh culture medium (15 min, 37°C, protected from light), washed with PBS, and suspended in 250 µL PBS. We measured the fluorescence at 488/530 nm

(H_2DCF-DA) and 514/580 nm (MitoSOX) using a FLUOstar Omega plate reader (Germany).

Intracellular metal concentration

We quantified intracellular concentrations of silver (Ag) and platinum (Pt) by inductively coupled plasma–mass spectrometry (ICP–MS; Bruker 820-MS + SPS 3 autosampler). Cells were seeded onto six-well plates, cultured for 24 h, and exposed to AgNP (3.5 µg/mL), CDDP (10 and 40 µM), or a combination of both, for 4 h. Subsequently, we washed the cells 3× with PBS (to remove AgNPs and CDDP from the cell surface), trypsinized (0.25% trypsin, 0.02% EDTA, in pH 7.2 PBS), harvested, and pelleted the cells in complete culture medium (500 *g* for 5 min). Pellets were further digested with 2% v/v HNO_3 overnight at room temperature and remained at −20°C until ICP–MS analysis. We used five-point calibration curves for quantification, and NIST 1486 (for the ICP–MS) for quality control. We performed three independent replicates; the results are expressed in ppm/10^3 cells.

Statistical procedures for biochemical and metal quantitation assays

We conducted three independent experiments with three replicates each for biomarkers analyzed in 96-well microplates and metal quantitation analysis. Data distribution was tested and parametric (one-way analysis of variance, ANOVA) tests were performed, followed by Dunnett's post-test. We verified the effects of treatments by a comparison of the control versus AgNPs, CDDP, or AgNPs/CDDP. Interaction effects induced by co-treatment with AgNPs/CDDP were identified by a comparison of the co-treatment group versus single-contaminant experiments that were performed in this study. We considered *p*-values less than 0.05 to be statistically significant.

Sample preparation for MS-based proteomics analysis

At the end of the treatment period, we discarded the culture medium and carefully washed the cells 3× with ice-cold PBS. Next, 1 mL of ice-cold PBS plus protease inhibitor (ProtoSTOP, Roche) was added to the plates and the cells were harvested with the aid of a cell scraper. We centrifuged the cell suspensions for 5 min at 600 *g* and discarded the supernatant. Cell pellets were stored at −80°C until further analysis.

We resuspended cell pellets in lysis buffer (6 M urea, 2 M thiourea, protease inhibitors, 20 mM triethylammonium bicarbonate, and 10 mM 1,4-dithiothreitol reducing agent) at room temperature for 2 h. Then, the urea concentration was diluted 10× and the cell lysis was enhanced by tip sonication on ice. We quantified proteins using Qubit fluorometric quantification (LifeTechnologies) and alkylated 50 µg of proteins in 20 mM iodoacetamide for 30 min in the dark. Following incubation, proteins were digested with trypsin (50:1 w/w protein:trypsin) overnight at room temperature. We acidified the peptide solution with 1 % v/v formic acid to stop trypsin digestion, and dried the peptides prior to desalting.

Desalting with R2/R3 microcolumns

Samples were resuspended in 0.1 % v/v trifluoroacetic acid (TFA) and desalted using self-made P200 columns, made with a C8 plug (Empore, 3M purification) packed with 1:1 Poros R2 and R3 (Applied Biosystems) resins materials in 100% acetonitrile (ACN). The column was prepared by applying a mild air pressure with a syringe and washing the column 2× with 0.1% v/v TFA. Subsequently, we loaded the acidified samples to the columns and washed them 2× with 0.1% v/v TFA. Peptides were eluted with 30% v/v ACN, 0.1% v/v TFA, followed by 70% v/v ACN, 0.1% v/v TFA.

Peptide labeling

We labeled tryptic peptides (50 µg per sample group) with the isobaric tag for relative and absolute quantitation (iTRAQ) 4-plex, in accordance with the manufacturer's protocol. For both cell lines, the tags used to label each experimental condition, in triplicate, were as follows: control (114), AgNPs (115), CDDP (116), and AgNPs/CDDP (117). We combined the peptides in a 1:1:1:1 ratio, dried them under vacuum, and stored them at −20°C until further processing.

Sample fractionation

To reduce complexity and remove unbound iTRAQ reagents, we pre-fractionated samples in an automated manner in reversed-phase at high pH, using a Dionex 3000 system (Thermo Fisher Scientific). Samples were solubilized in buffer A (20 mM ammonium formate, pH 9.2) and the column was loaded. Finally, we eluted the peptides at 100 nL/min by increasing buffer B (80% v/v ACN and 20% v/v buffer A) from 2% to 50%, over 85 min. We sampled 20 fractions, which we concatenated into 10 fractions. These samples including the flow-through were then dried in a vacuum centrifuge.

Reversed-phase nano-liquid chromatography–tandem MS

We resuspended each high-pH fraction in 0.1% v/v formic acid (FA) and loaded them on an in-house packed trap column (3-cm × 100-µm inner diameter; 5 µm) filled with ReproSil-Pur C18 AQ (Dr. Maisch, Ammerbuch–Entringen, Germany). Peptides were separated on an analytical column (18-cm × 75-µm inner diameter; 3 µm) packed in-house with ReproSil-Pur C18 AQ (Dr. Maisch, Ammerbuch-Entringen, Germany), by reversed-phase chromatography on an EASY-nanoLC system (Thermo Fisher Scientific).

The chromatography gradient was as follows: 0% to 3% B for 3 min, 3% to 25% B for 80 min, 25% to 45% B for 15 min, 45% to 100% B for 3 min, followed by 8 min in 100% B (A: 0.1% v/v FA; B: 95% v/v ACN, 0.1% v/v FA) at a constant flow rate of 250 nL/min. We connected the Easy-nanoLC system online to a Q Exactive high-field hybrid quadrupole–orbitrap mass spectrometer (Thermo Fisher Scientific) operating in positive ion mode using data-dependent acquisition. The Orbitrap acquired the full scan with an automatic gain control target value of 3×10^6 and a maximum injection time of 100 ms. We acquired each mass spectrometer scan at a resolution of 60,000 at an *m*/*z* 200 with a mass range of *m*/*z* 400–1600. We subjected the 20 most-intense precursor ions (charge from 2 to 5) to higher-energy collisional dissociation fragmentation. Fragmentation was performed at a normalized collisional energy of 30% using an isolation width of 1.2 Da and a dynamic exclusion duration of 20 s. We acquired tandem mass spectrometry (MS^2) spectra at 30,000 resolution, *m*/*z* 200, with an automatic gain control of 1×10^5 and a maximum injection time of 200 ms.

Database search and bioinformatics analyses

We processed raw data using Proteome Discoverer v2.1.1.21 (Thermo Fisher Scientific) and searched against the SwissProt human database using the Mascot search engine. Trypsin was chosen as the enzyme, allowing two missed cleavage sites. We used a precursor mass tolerance of 10 ppm and a product ion mass tolerance of 0.02 Da. Fixed modifications included carbamidomethylation of cysteines and iTRAQ4-plex labeling for lysines and N-termini. Dynamic modifications contained methionine oxidation and N-terminal acetylation. We calculated false discovery rates using the Percolator algorithm (*q*-value filter set to 0.01). Quantification was performed using the Proteome Discoverer workflow node “Reporter Ions quantifier” on the log2-values of the measured normalized

peptide abundances. We determined protein regulations using the Limma ranked-product approach (18). Only proteins with *p*-values ≤ 0.01 were considered to be regulated. We submitted regulated proteins to Ingenuity Pathway Analysis (IPA; Quiagen) to elucidate cellular protein responses induced by exposure to the contaminants, and to the Search Tool for the Retrieval of Interacting Genes/Proteins (STRING) app from Cystoscope to reveal protein–protein interactions (19).

Results and discussion

AgNP characterization

Dynamic light scattering measurements indicated that the AgNP suspension had a major peak with a mass distribution of approximately 10 nm (Figure 1A). The zeta potential of the sample was −38.9 mV ± 1.75 mV, measured for AgNPs dispersed in the citrate buffer with the addition of 1 mM KCl, indicating good colloidal nanoparticle stability (data not shown). Nanocomposix provided the transmission electron microscopy images, which confirmed that the AgNPs were monodisperse and spherical (Figure 1B).

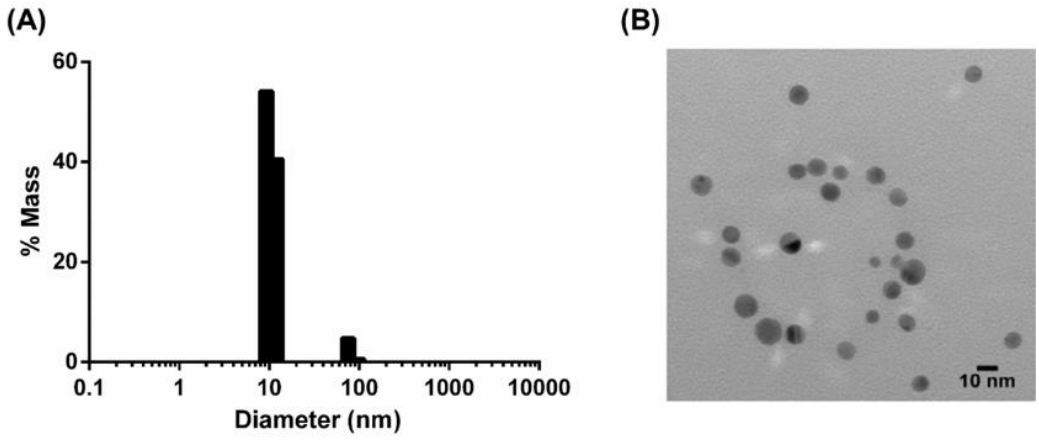

Figure 1. Silver nanoparticle (AgNP) characterization. (A) Particle distribution in accordance with size. (B) Transmission electron microscopy image of the AgNP suspension.

AgNPs/CDDP combination induces toxicological interaction in HepG2 cells

We performed toxicity screening based on MTT metabolism in HepG2 cells. We applied various concentrations of AgNPs (0–10 µg/mL) and CDDP (0–200 µM) for 24 h, to select the concentrations to be tested for drug interaction assays (Figure 2A). Based on these results, we selected three concentrations of AgNPs (1 µg/mL, no toxicity; 3.5 µg/mL, ≈ 30% viability loss; and 5 µg/mL, ≈ 50% viability loss) and two concentrations for CDDP (10 µM, no toxicity; and 40 µM, ≈ 30% viability loss) to study the cytotoxic interaction of AgNPs and CDDP.

These results indicate that 3.5 µg/mL AgNPs in combination with both nontoxic and moderately toxic concentrations of CDDP generate an interaction effect (i.e., higher than the sum of the toxicity induced by single treatments), which significantly lessened the viability of HepG2 cells (Figure 2B). To date, only a few studies have investigated the ability of AgNPs to enhance the toxicity caused by conventional chemotherapy. Combining AgNPs with doxorubicin is efficient against breast and liver cancer (20,21), due to increased cytotoxicity and ROS levels. AgNPs together with salinomycin or gemcitabine leads to enhanced apoptosis, oxidative stress, and cytotoxicity in ovarian cancer cells (22,23). Kovács and coworkers investigated AgNPs combined with several antineoplastic drugs and found, for all test combinations, synergy against adenocarcinoma cells (14). These studies indicate the promising potential of AgNPs as a combinatorial agent for chemotherapy. However, researchers do not fully understand how this

toxicological interaction occurs in detail and particularly how normal cell lines respond to such combinatorial treatment.

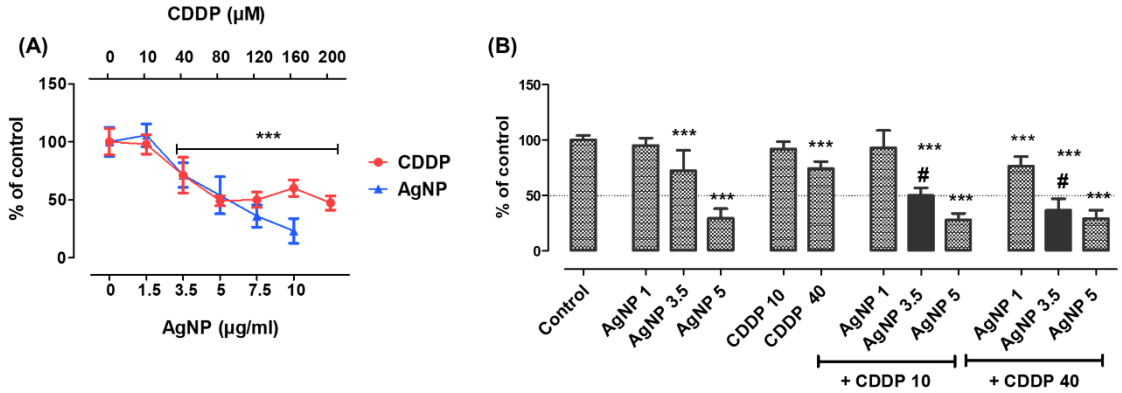

Figure 2. Toxicity screening. (A) MTT assay performed in HepG2 cells after 24 h of treatment with AgNPs (0–10 µg/mL) or CDDP (0–200 µM). (B) MTT assay performed in HepG2 cells after 24 h of treatment with AgNPs (1–5 µg/mL), CDDP (10 or 40 µM), and corresponding combinations. Mean + standard deviation (SD) of three independent experiments in triplicate. Asterisks indicate difference in comparison to the control (***p<0.001); sharp symbol (#) indicates toxicological interaction.

HepG2 cells are more susceptible to AgNPs/CDDP than THLE2 cells

We evaluated the effects of AgNPs, CDDP, and corresponding combinations on cell viability and ROS levels, in both tumoral (HepG2) and normal (THLE2) cell lines after 24 h of treatment (Figure 3).

We assessed the cytotoxicity of AgNPs, CDDPs, and AgNPs/CDDP by an MTT metabolism assay (Figure 3A). Single treatment with AgNPs was more harmful to HepG2 cells (30% viability loss) than to THLE2 cells (no viability loss). In contrast, CDDP had more of an effect on THLE2 cells than HepG2 cells: 10 µM CDDP led to 10% viability loss in HepG2 cells and ≈ 25% loss in THLE2 cells, while 40 µM CDDP led to ≈ 25%

viability loss in HepG2 cells and ≈ 70% viability loss in THLE2 cells. The combinatorial effect of AgNPs/CDDP led to a higher toxicity than single treatments for both cell lines, and we observed toxicological interaction in most groups. Particularly interesting was the treatment with AgNPs and the lower concentration of CDDP (10 µM). Whereas the combination of drugs led to a 50% decrease in the viability of HepG2 cells, normal THLE2 cells were notably less hindered, losing ≈ 20% of their viability. Using a higher concentration of CDDP (40 uM) equalized the response to the exposure between the cell lines, thus exceeding the threshold for hindering the cancerous cell line compared to the normal cell line.

We quantitated ROS levels in the cytosol and mitochondria (Figures 3B and 3C). Single treatments with AgNPs and 10 µM CDDP increased ROS in neither HepG2 nor THLE2 cells. Treatment with 40 µM CDDP was toxic to THLE2 cells, leading to a 90% increase in cytosolic H_2O_2 (Figure 2B) and a 190% increase in mitochondrial superoxide (Figure 2C). Combinations of AgNPs and CDDP induced a toxicological interaction in HepG2 cells, whereas normal cells were resistant to the combination with the lowest CDDP concentration. Thus, regarding biological endpoints, cell viability, and ROS levels, tumoral HepG2 cells were more sensitive to the combined exposure of AgNPs and 10 µM CDDP than normal THLE2 cells.

Due to their fast metabolism, tumoral cells generate higher ROS levels compared to normal cells. Although this characteristic is protumorigenic, it also renders tumoral cells more susceptible to oxidative stress-induced damage than normal cells, once a tolerance level is reached sooner (24). Researchers have well-documented that an increased level of ROS is one of the main outcomes after exposure to AgNPs. Therefore, it is possible that co-exposure with AgNPs contributed to the high toxicity observed in tumoral HepG2 cells treated with AgNPs/CDDP. However, normal THLE2 cells

maintained ROS at tolerable levels and resisted initiating cell death when treated with AgNPs and a non-cytotoxic concentration of CDDP (10 mM). In accordance with our findings, a recent study has shown that tumoral HepG2 cells undergo higher levels of apoptosis than normal LO2 cells after treatment with AgNPs and paclitaxel, which was related to oxidative stress (25). These findings support that normal cells are more resistant to ROS-mediated cell damage than tumoral cells, upon treatment with AgNPs.

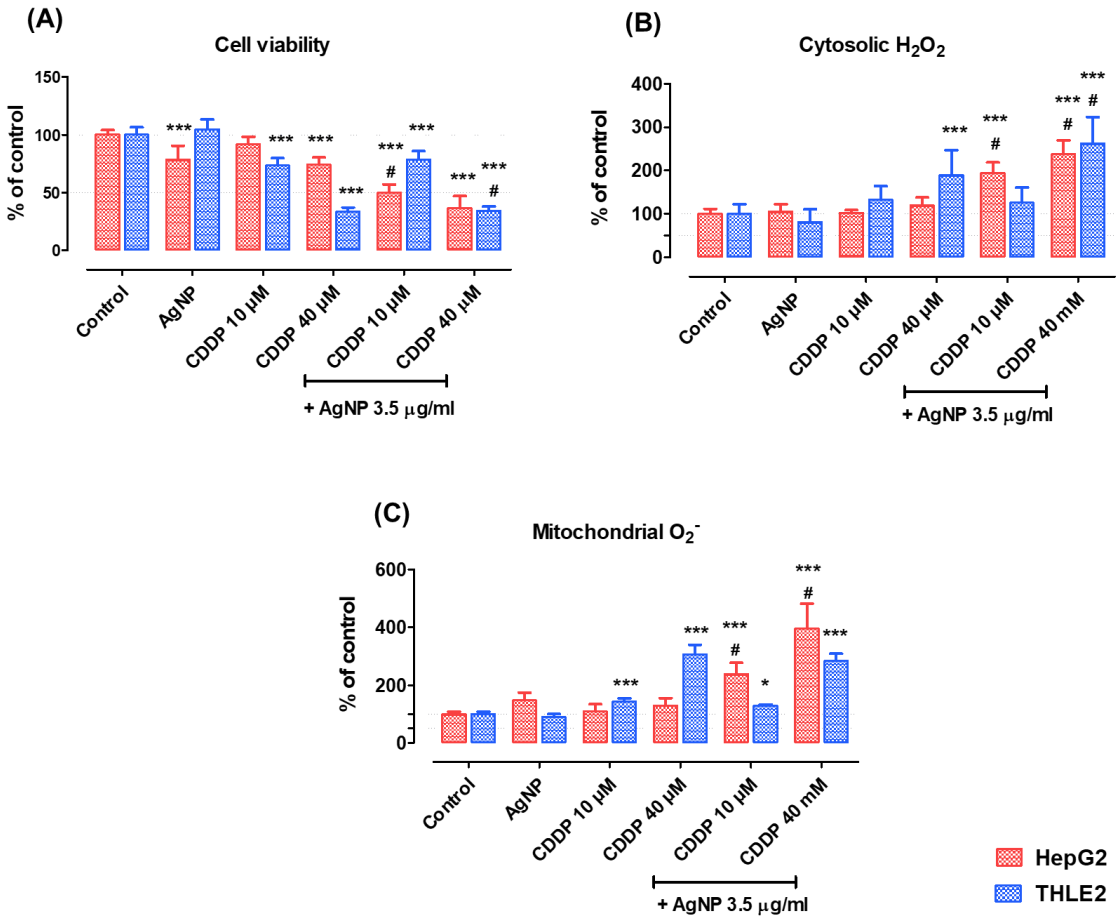

Figure 3. Biological endpoints. (A) Cell viability, (B) cytosolic hydrogen peroxide levels, and (C) mitochondrial superoxide levels in HepG2 and THLE2 cells treated for 24 h with AgNPs (3.5 µg/mL), CDDP (10 or 40 µM), or AgNPs/CDDP (3.5 µg/mL and 10 or 40 µM CDDP). Mean + SD of three independent experiments in triplicate. Asterisks indicate

difference in comparison to the control (*p<0.05, ***p<0.001); sharp symbol (#) indicates toxicological interaction.

Influence of AgNPs on CDDP cellular uptake

We performed ICP–MS analysis to investigate whether the higher toxicity observed in cells treated with combinations of AgNPs and CDDP correlated to intracellular uptake, by measuring concentrations of Ag and Pt. Analysis in HepG2 cells revealed that the Pt concentration doubled in the presence of AgNPs (Figure 4A). In contrast, we observed no significant changes in intracellular concentrations in neither Ag nor Pt after the combined treatment of AgNPs/CDDP in THLE2 cells (Figure 4B).

These results suggest that the toxicological interactions observed after combinatorial treatment in HepG2 may, at least in part, be explained by increased CDDP intracellular accumulation. Based on previous studies, we hypothesize that increased levels of CDDP in HepG2 cells might be related to multidrug resistance to transporter activity. Analogously to several antineoplastic drugs, multidrug resistance transporters pump CDDP to the extracellular environment, and thus play an important role in tumor resistance to chemotherapy (26). AgNPs can interfere with the activity and expression of these proteins (13,14), which could possibly lead to intracellular accumulation of chemotherapy drugs.

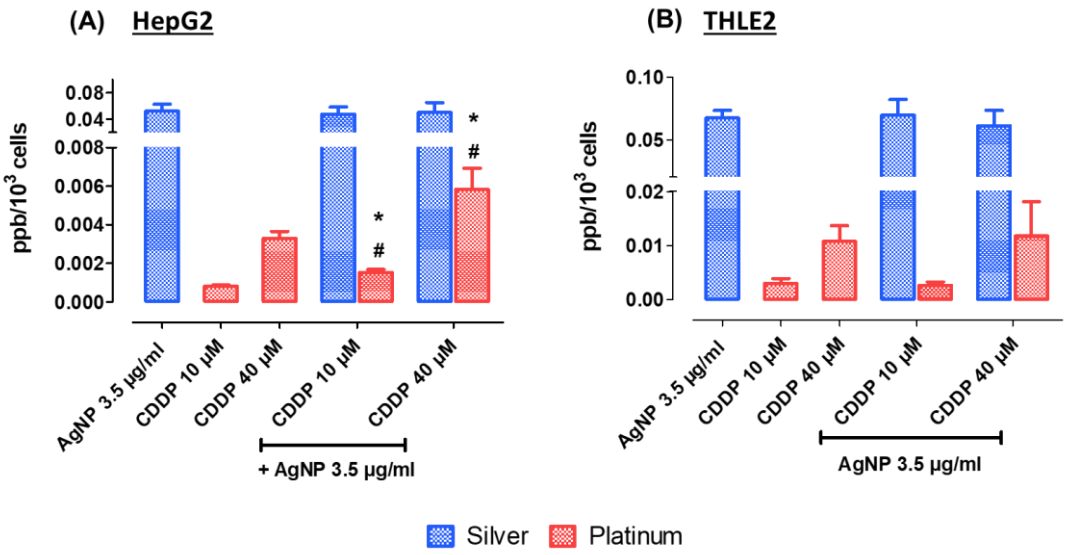

Figure 4. Intracellular concentrations of Ag and Pt in (A) HepG2 cells and (B) THLE2 cells treated for 4 h. Results are expressed in ppm/10^3 cells. Mean + SD of three independent experiments. Asterisks indicate difference in comparison to the correspondent metal uptake for single exposures (*p<0.05); sharp symbol (#) indicates toxicological interaction.

Proteomics analysis

To identify molecular pathways involved in the cellular outcomes induced by AgNPs/CDDP (3.5 µg/mL + 10 µM), we conducted quantitative proteomics after 24 h of treatment. For HepG2 and THLE2 cells, we quantitated 5,694 and 6,380 proteins, respectively, with at least three unique peptides based on iTRAQ reporter ion intensities. We considered only proteins with p-values less than 0.01 to be regulated (Figure 5 and additional file 1: figure 1).

In this study, upregulated refers to proteins that were more abundant in comparison to the control, whereas downregulated refers to proteins that were less abundant compared to the control. Figure 5 shows the number of deregulated proteins after 24 h of treatment

with AgNPs, CDDP, and their corresponding combinations in HepG2 and THLE2 cells (for details on protein ID and quantitation see additional files 2 and 3). Treatment with AgNPs resulted in 1,154 deregulated proteins, of which 455 were upregulated and 699 were downregulated in HepG2 cells, whereas in THLE2 cells no proteins were deregulated. Treatment with CDDP resulted in 433 upregulated and 540 downregulated proteins for HepG2 cells; for THLE2 413 proteins were upregulated and 425 proteins were downregulated. A combination of these two substances resulted in deregulation of 2,969 proteins (≈ 50% of the measured proteome) in HepG2 cells, of which 1,331 were upregulated and 1,638 were downregulated. THLE2 cells also exhibited deregulation of several proteins, accounting for a total of 1,393 proteins (≈ 20% of the proteome), of which 751 were upregulated and 642 were downregulated.

For both cell lines, proteome changes followed a similar trend as that observed in cell viability assays (Figure 3A). Specifically, the proteome deregulation observed after AgNPs/CDDP treatment was larger than the sum of the two single treatments. However, this effect was substantially enhanced in HepG2 cells compared to THLE2 cells.

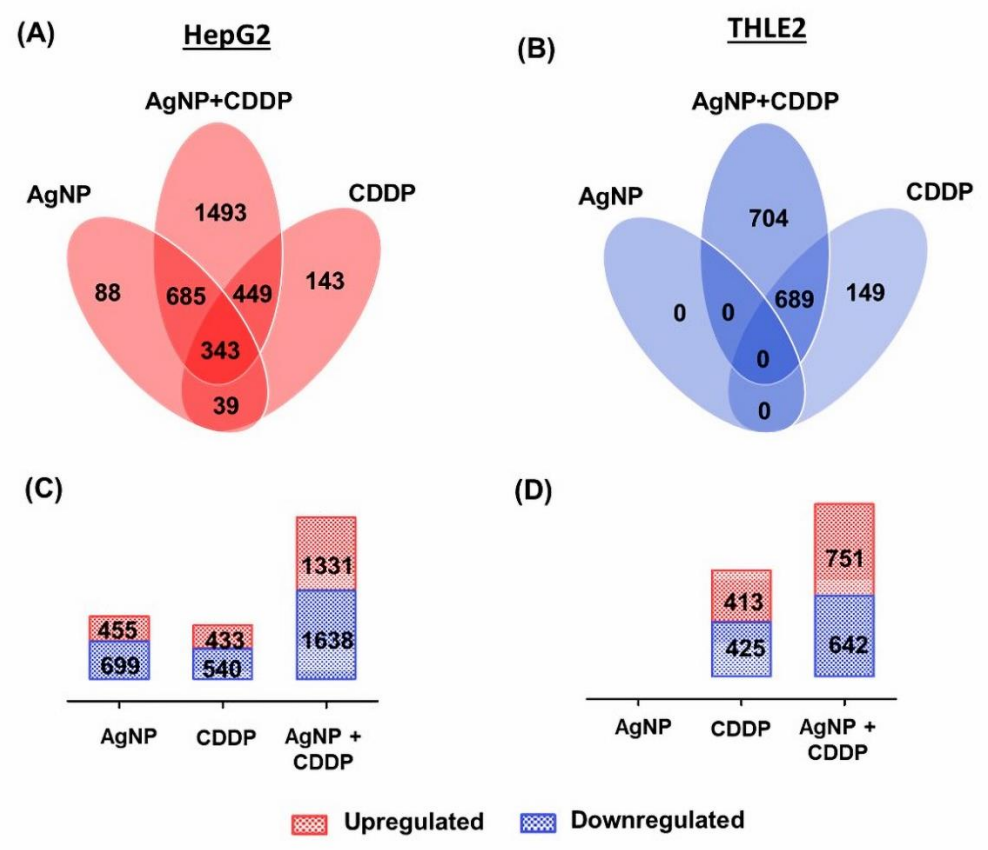

Figure 5. Quantitative data of proteomic analysis of three independent experiments, after both cell lines were exposed for 24 h to AgNPs (3.5 µg/mL), CDDP (10 µM), and AgNPs/CDDP (3.5 µg/mL + 10 µM). We quantitated a total of 5,694 proteins in HepG2 cells and 6,380 proteins in THLE2 cells, in all experimental conditions. We built Venn diagrams to examine the profiles of protein deregulation by overlapping the treatment conditions in (A) HepG2 cells and (B) THLE2 cells. (C) Regulated proteins in HepG2 cells. (D) Regulated proteins in THLE2 cells.

AgNPs/CDDP combination affects similar pathways and upstream regulators in HepG2 and THLE2 cells

To reveal the main molecular pathways disturbed after 24-h treatments for both cell lines, we performed canonical pathway and upstream regulator analyses, using IPA software.

For HepG2 cells (Figure 6A), among the top 10 canonical pathways affected by AgNPs/CDDP, half were related to energy metabolism (mitochondrial dysfunction, oxidative phosphorylation, glycolysis, the TCA cycle, and fatty acid β-oxidation), and two were related to stress resistance (Nrf-2 regulation and the sirtuin signaling pathway). The actin cytoskeleton, cell signaling, and protein ubiquitination canonical pathways were also significantly disturbed. Regarding single treatments, AgNP outcomes were mostly associated with the response to oxidative stress and energy metabolism (glycolysis and the TCA cycle), whereas treatment with CDDP was also associated with energy metabolism (mitochondrial dysfunction and oxidative phosphorylation), as well as the cytoskeleton and stress response (the sirtuin signaling pathway).

For THLE2 cells (Figure 6B), it is notable that CDDP and AgNPs/CDDP disturbed similar pathways. The majority of the top 10 canonical pathways were associated with energy metabolism (mitochondrial dysfunction, oxidative phosphorylation, the TCA cycle, fatty acid β-oxidation, ketogenesis, acetyl co-A biosynthesis, and amino acid degradation); protein ubiquitination, stress resistance, and RAN signaling pathways were also affected.

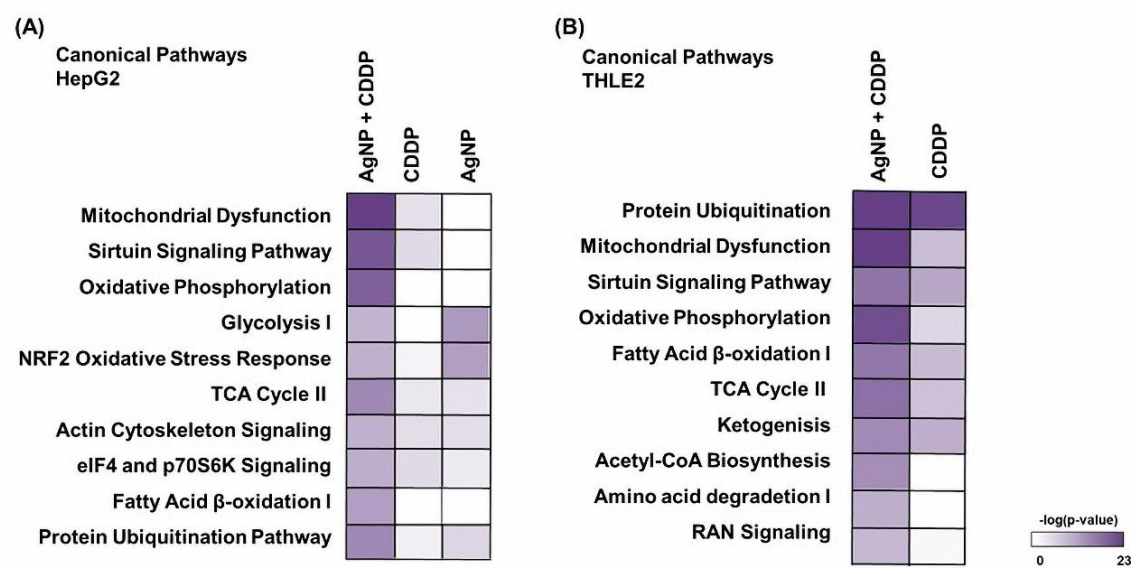

405

406

407 Figure 6. Ingenuity pathway analysis, a canonical pathway analysis. Top 10 significantly
408 affected [−log(*p*-value) ≥ 1.3] pathways in (A) HepG2 cells and (B) THLE2 cells after 24
409 h of exposure to AgNPs/CDDP. The corresponding −log(*p*-value) of these canonical
410 pathways is also represented for single treatments.

411

412 We compared the top canonical pathways of both cell lines treated with
413 AgNPs/CDDP (Figure 7B). Similar pathways were affected in both cell lines, except for
414 glycolysis, the nucleotide excision and repair (NER) pathway, the NRF2 stress response
415 pathway, actin, and eif4 signaling, which were only significantly disturbed in HepG2
416 cells.

417 Figure 7C shows upstream regulators (*z*-score ≥ 2 or ≤ −2) involved in protein
418 deregulation following exposure to AgNPs/CDDP. Eight upstream regulators followed
419 the same activation pattern in both cell lines after treatment with AgNPs/CDDP. Among
420 these, six are related to energy metabolism (PPARGC1A, PPARA, SRBP1, SRBP2,
421 MLXIP, and FOXO1), whereas others are related to the DNA damage response and cell

cycle arrest [breast cancer type 1 susceptibility protein (BRCA1)], and histone demethylase (KDM5A).

Activated upstream regulators upon AgNPs/CDDP treatment that we observed only in HepG2 cells are RB1, which is a key regulator of cell cycle arrest; FOXO3, which is a transcriptional activator involved in apoptosis regulation in response to oxidative stress; and KLF15. SIRT2 was the only inhibited upstream regulator that we observed exclusively in HepG2 cells; this protein has a central role in cell cycle progression and genomic stability.

For THLE2 cells, NRF2 (a key transcriptional activator of genes related to the response to oxidative stress) and NFKBIA (an inhibitor of the activity of the complex NF–Kβ/REL) were indicated as active upstream regulators after AgNPs/CDDP treatment. MTPN (promotes dimerization of NF–Kβ subunits, regulates corresponding transcriptional activity, and has a role in actin filament dynamics) was indicated as an inhibited upstream regulator.

AgNPs/CDDP treatment altered similar pathways and upstream regulators in both cell lines. Energy metabolism, response to oxidative stress, and regulation of cell fate were common targets after co-treatment.

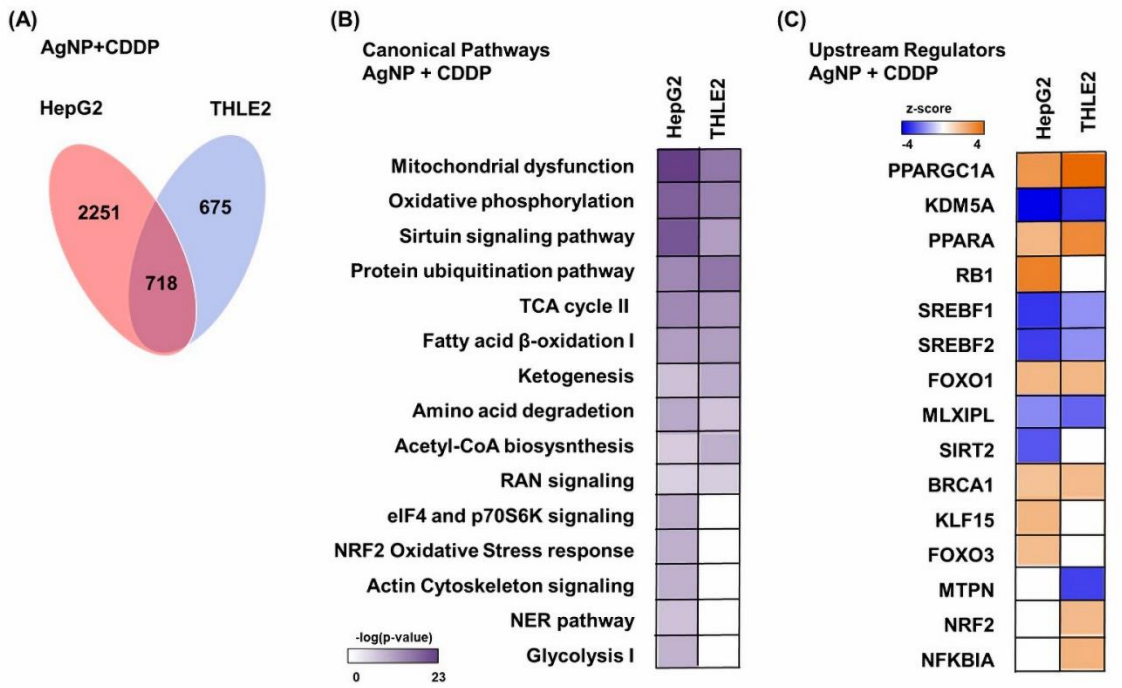

Figure 7. Venn diagram built to show proteins deregulated by AgNPs/CDDP overlap in both cell lines. (A) Number of proteins uniquely deregulated: HepG2 cells, 2215 proteins; THLE2 cells, 675 proteins; 718 proteins were in common deregulated in both cell lines. (B) Comparison of main significantly affected [−log(*p*-value) ≥ 1.3] canonical pathways between HepG2 and Thle2 cell lines, after AgNPs/CDDP treatment, indicated by IPA software. (C) Top active (*z*-score ≥ 2) and inactive (*z*-score ≤ −2) upstream regulators in HepG2 and THLE2 cells after 24 h of exposure to AgNPs/CDDP indicated by IPA software.

AgNPs/CDDP treatment induces energy metabolism adaptation

The metabolism of tumoral cells differs substantially from normal cells because the metabolism of the former is adapted for fast growth in hypoxic and acidic environments. Therefore, glycolysis is the preferred pathway to synthesize ATP, even in the presence of oxygen and functional mitochondria, because glycolysis generates energy more rapidly

than oxidative phosphorylation (27,28). For this reason, cancer energy metabolism has gained attention in relation to cancer treatment. The glycolysis pathway was significantly enriched in HepG2 cells, with all main proteins involved being downregulated after exposure to AgNPs alone and AgNPs/CDDP (Figures 6A, 8E, and additional file 1: table 2). This information shows that AgNPs impair an important cancer hallmark and that combining them with CDDPs increases this effect somewhat further.

In proliferating normal or tumoral cells, glucose is an essential nutrient for supplying cells with energy (29,30). However, under nutrient deprivation, alternative energy sources such as fatty acids, glutamine, and proteins may be oxidized through the TCA cycle and fatty acid β-oxidation to generate ATP (31,32). NADH and $FADH_2$ generated in these processes are used during oxidative phosphorylation to reduce molecular oxygen to water and generate ATP.

The TCA cycle, fatty acid β-oxidation, amino acid degradation, and oxidative phosphorylation canonical pathways were significantly affected after AgNPs/CDDP treatment in both cells (Figure 7B); the majority of the proteins related to these pathways were upregulated (Figures 8A–D). These outcomes suggest that both cell lines may have used alternative nutrients to supply metabolic demand, such as the lipids and amino acids present in the complete culture medium.

In HepG2 cells, not only did AgNPs/CDDP hinder glycolysis, the combination also led to decreased GLUT 1 levels (see additional file 2: page 98, accession number P11166), the main glucose carrier in HepG2 (33). An inability to efficiently take up and metabolize glucose through glycolysis may have induced the cells to adapt and increase other energy-generating pathways. This adaptation, however, was insufficient to avoid cell death. For THLE2 cells, metabolic adaptation may have contributed to a lower

480 percentage of cell death (20%) compared to HepG2 cells (50%), after treatment with
481 AgNPs/CDDP (Figure 3A).

482 Peroxisome proliferator-activated receptor alpha (PPARA) and peroxisome
483 proliferator-activated receptor gamma coactivator 1-a (PPARGC1A) are active upstream
484 regulators in both cell lines after AgNPs/CDDP treatment. PPARA is a key regulator of
485 lipid metabolism; in particular, peroxisomal fatty acid β-oxidation (34); whereas
486 PPARGC1A plays an essential role in metabolic reprogramming in response to nutrient
487 availability, coordinating the expression of genes involved in glucose and fatty acid
488 metabolism (35). Therefore, activation of these upstream regulators may be related to the
489 upregulation of the TCA cycle and fatty acid β-oxidation pathways.

490 Key regulators of lipid synthesis, sterol regulatory element-binding protein
491 (SREBP-1 and 2), and carbohydrate-responsive element-binding protein (MLXIPL, also
492 known as ChREBP) were inhibited in both cell lines after AgNPs/CDDP treatment. These
493 transcriptional activators are essential for lipogenesis and its inhibition may be associated
494 with the cellular energetic state (36–38).

495 Our findings suggest that treatment with AgNPs/CDDP affects energy homeostasis,
496 and the cells respond by increasing alternative nutrient catabolic processes and inhibiting
497 anabolic processes related to energy storage.

498

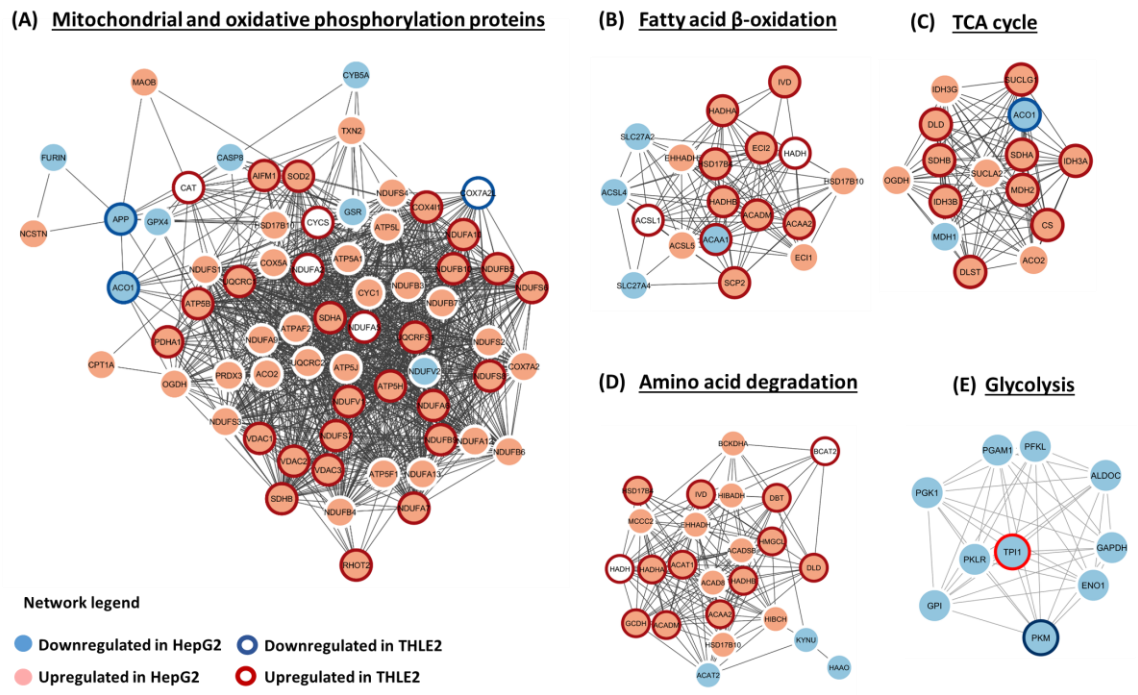

Figure 8. Protein–protein interaction networks of energy metabolism canonical pathways affected by AgNPs/CDDP treatment in HepG2 and THLE2 cells. We built functional interaction networks of deregulated proteins of each pathway with the STRING algorithm. Lines represent interactions and only interactions with medium confidence (score ≥ 0.4) are shown. Upregulated proteins in HepG2 cells are light red, whereas downregulated proteins are light blue. For THLE2 cells, a dark red halo around a protein indicates that the protein is upregulated, whereas a dark blue halo indicates that the protein is downregulated.

AgNPs/CDDP treatment affects cell proliferation

The sirtuin signaling pathway regulate many physiological processes, ranging from energy metabolism to epigenetic modifications (39–41). The pathway was significantly affected in both cell lines after AgNPs/CDDP treatment (Figure 7B). We grouped proteins associated with this canonical pathway into two main clusters (Figure 9). Cluster 1

515 comprises several upregulated proteins associated with mitochondrial energy
516 metabolism, whereas cluster 2 comprises several downregulated proteins related to cell
517 cycle control such as MAPK 1 and 3, AKT1, MTOR, RPTOR (most of which were only
518 deregulated in HepG2 cells), and the tumor suppressor TP53, which is upregulated in both
519 cells.

520 Two upstream regulators related to cell cycle control exhibited similar activation
521 states in both cell lines after AgNPs/CDDP treatment. BRCA1, an E3 ubiquitin-protein
522 ligase that acts as a tumor suppressor, is involved in DNA damage repair and promotes
523 cell cycle arrest in response to DNA damage (42,43). Lysine-specific demethylase 5A
524 (KDM5A, also termed RBP2) is a potential oncogene that is highly expressed in many
525 different cancers (44). Due to its demethylase activity, this protein activates cell growth
526 by decreasing the expression of cell cycle inhibitors and affecting cell cycle arrest by
527 forming complexes with multiple proteins to regulate transcriptional activation.(45,46)
528 BRCA1 and KDM5A are, respectively, activated and inactivated in both cell lines after
529 AgNPs/CDDP treatment. This suggests that both cells lines responded to DNA damage
530 and arrested cell proliferation. For HepG2 cells, although BRAC1 is activated and
531 possibly stimulates DNA repair, the NER pathway was significantly disturbed (Figure
532 7B). Several proteins belonging to this pathway were downregulated (Additional file 1:
533 table 3) after co-treatment, thus possibly leading to genomic instability and consequently
534 reduced cell viability.

535 In addition to BRCA1 and KDM5A, retinoblastoma-associated protein (RB1) was
536 also an active upstream regulator in HepG2 cells after AgNPs/CDDP treatment. The non-
537 phosphorylated active form of this protein acts as a tumor suppressor by limiting the
538 transcription of cell cycle genes, mainly via regulation of the E2F transcription factor
539 (47).

Our data suggests that both cell lines inhibited anabolic processes such as cell proliferation, and stimulated catabolic processes dramatically to overcome the energetic stress induced by AgNPs/CDDP treatment.

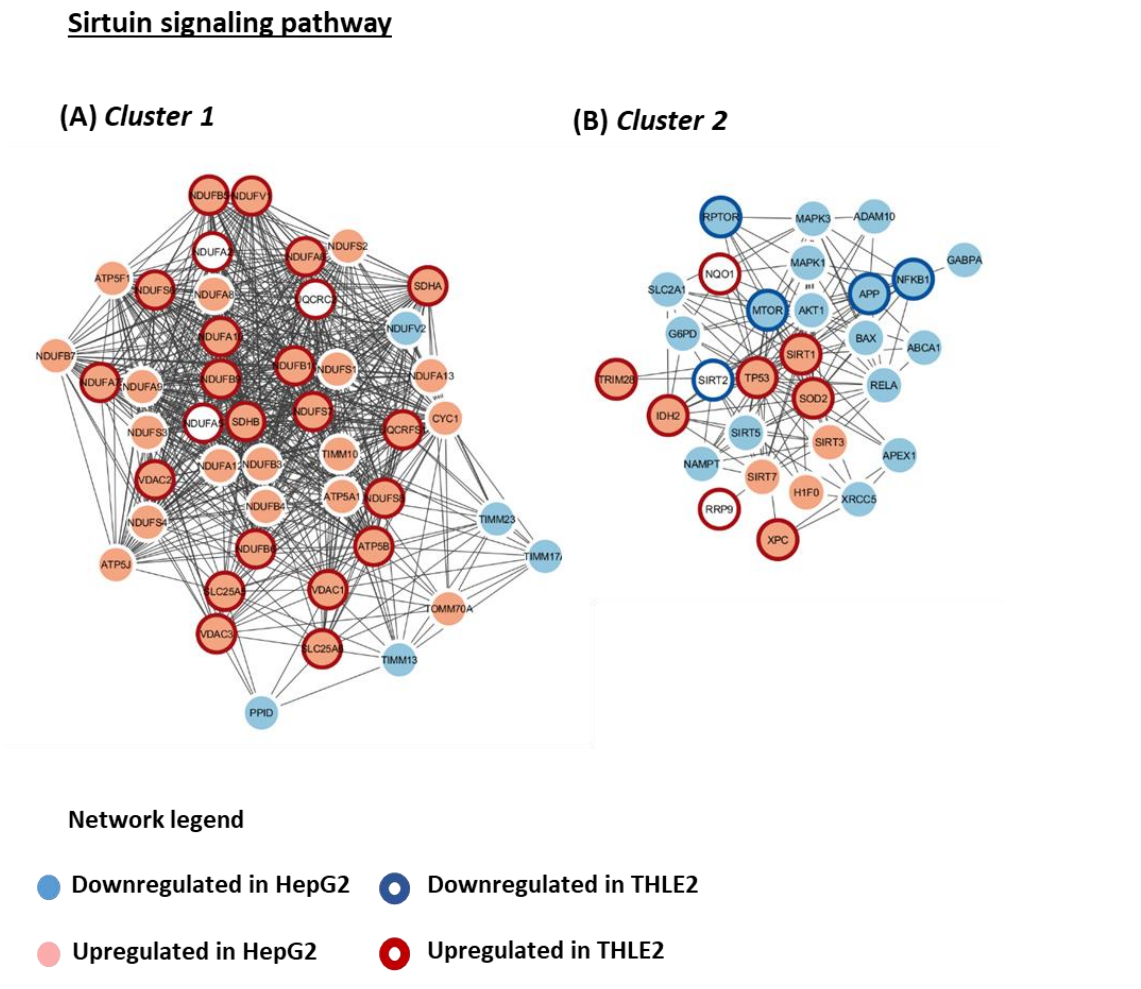

Figure 9. Protein–protein interaction networks of the sirtuin canonical pathway affected by AgNPs/CDDP treatment in HepG2 and THLE2 cells. We built functional interaction networks of deregulated proteins of each pathway with the STRING algorithm. Lines represent interactions and only interactions with medium confidence (score ≥ 0.4) are shown. We used the Markov cluster algorithm (MCL) to identify clusters of tightly connected proteins within the network. Upregulated proteins in HepG2 cells are light red,

whereas downregulated proteins are light blue. For THLE2 cells, a dark red halo around a protein indicates that the protein is upregulated, whereas a dark blue halo indicates that the protein is downregulated.

Oxidative stress is enhanced in tumoral cells after AgNPs/CDDP treatment

Oxidative stress results from an imbalance between ROS and antioxidant defenses, to detoxify ROS intermediates or repair the resulting damage. Cells respond by increasing the transcription and activity of antioxidant proteins, and by activating pathways to promote cell survival and manage with the stress response (48). NRF2 is a transcription factor that regulates basal and inducible expression of antioxidant response genes, thus playing a key role in cellular redox homeostasis. The cytoplasmic protein Keap1 interacts with NRF2 and represses its function under homeostatic conditions. When intracellular ROS levels increase, this complex dissociates and NRF2 translocates into the nucleus, promoting transcription of antioxidant genes (49,50).

This scenario seems to be how normal THLE2 cells respond to treatment with AgNPs/CDDP. Although the NRF2 pathway was not significantly affected by the co-treatment, the transcription factor NRF2 was activated in these cells (Figure 7). This activation possibly led to upregulation of several antioxidant proteins, such as NAD(P)H:quinone acceptor oxidoreductase 1 (NQO1), heme oxygenase-1 (HMOX1), and thioredoxin reductase (TXNRD2). Catalase, peroxirredoxin (both of which are important enzymes that help reduce hydrogen peroxide), and superoxide dismutase (destroys superoxide anion radicals) were also upregulated (Figure 10). These outcomes might have resulted in the maintenance of ROS at control levels after treatment with AgNP + 10 μM CDDP (Figures 3B and 3C) and the low cytotoxicity (Figure 3A).

AgNPs and AgNPs/CDDP induced a different response in HepG2 cells. In these cases, the NRF2-mediated stress response was significantly affected (Figure 6A, additional file1: table. 4). For AgNPs/CDDP treatment, downregulation of several antioxidant proteins occurred (Figure 10); in particular, the proteins involved in the metabolism of glutathione, one of the main intracellular ROS scavengers. These were glutathione synthetase (GSS), glutathione S-transferase (GSTA1, GSTO1, and GSTM3), and glutathione peroxidase (GPX). Thioredoxin (TXN) was also downregulated after AgNPs/CDDP treatment. This enzyme participates in protein repair after oxidative damage and is responsible for reducing oxidized proteins, including peroxirredoxin, which was also downregulated.

The reduction of the antioxidant pool is possibly related to the increased ROS levels induced by AgNPs alone and together with CDDP (Figures 3B and 3C), and may play a key role in decreased cell viability (Figure 3A).

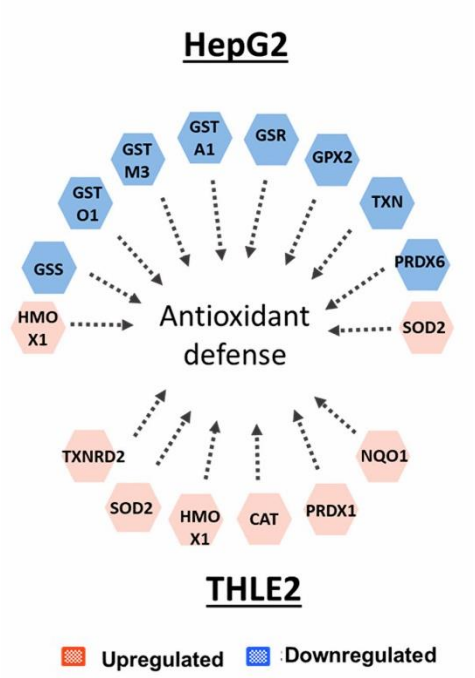

Figure 10. Antioxidants protein deregulated after treatment with AgNPs/CDDP in HepG2 and THLE2 cells.

Conclusions

Our results demonstrate the efficacy of AgNPs as a combinatorial agent to enhance the biological effect of CDDP, in both tumoral and normal cells. We performed quantitative MS-based proteomic, metal quantification, and biological endpoints assays to achieve deeper understanding on the effect of this combination in HepG2 and THLE2 cells. Biochemical endpoints showed that the toxicological interaction of AgNPs/CDDP occurred in both cell lines; however, the effect was more pronounced in HepG2 cells. This might, at least to some extent, be related to increased CDDP intracellular accumulation after the co-treatment. Proteomics analyses revealed that energy metabolism-related pathways were significantly affected in both cell lines. Upregulation of proteins related to the TCA cycle, fatty acid β-oxidation, amino acid degradation, and oxidative phosphorylation indicates that both cells lines possibly underwent energy stress due to AgNPs/CDDP treatment, and alternative nutrient degradation pathways were activated to supply cellular ATP demand. It is possible that energetic demand was higher for HepG2 cells due to downregulation of main glycolytic proteins. Canonical pathways and upstream regulators related to cell proliferation showed protein downregulation and inactivation, respectively, indicating reduced cell proliferation. The oxidative stress response differed in both cell lines. Whereas a downregulation of antioxidant proteins occurred in HepG2 cells, THLE2 cells exhibited upregulation of its antioxidant defense system. Although both cell lines were hindered by AgNPs/CDDP treatment, the response of the normal THLE2 cells was more successful in avoiding cell death than that of HepG2

cells. Taken together, our results indicate that a combination of AgNPs and CDDP has great potential for clinical applications.

Ethics approval and consent to participate

Not applicable.

Consent for publication

All authors consent to publish.

Availability of data and materials

The datasets used and/or analysed during the current study are available from the corresponding authors on reasonable request.

Competing interests

The authors declare that they have no competing interests

Authors' contributions

RM: Designed the experiments, conducted most of the experimental work [e.g., cell culture maintenance and treatments, biochemical assays, sample preparation for all analyses (MS, inductively coupled plasma, and particle characterization), MS runs, data searches, statistical analyses, and pathway analyses], analyzed all data, prepared all figures and tables, and wrote the manuscript. **MPF:** Contributed with high-pH fractionation, MS runs, data searches and statistical analyses for proteomics. **BK:** Conducted DLS and zeta potential measurements. **LS** and **KL:** Conducted inductively coupled plasma measurements. **FK:** Designed the experiments; contributed to the writing

641 of the manuscript, data analyses and interpretation. All authors read and approved the
642 final manuscript.
643
644 **Acknowledgments and Funding**
645 We acknowledge financial support by the European Research Council (ERC) under
646 the European Union's Horizon 2020 Research and Innovation Programme (grant
647 agreement no. 646603), and the VILLUM Center for Bioanalytical Sciences at the
648 University of Southern Denmark.
649
650 **References**
651
652 1 Hoyt VW, Mason E. Nanotechnology Emerging health issues. *J Chem Heal Saf*
653 2008; 15: 10–15.
654 2 Andreani T, Severino P, de Hollanda LM, Vazzana M, Souto SB, Santini A, Silva
655 AM, Souto EB. In *Nanostructures for Cancer Therapy*. Elsevier, 1st edition,
656 chapter 9; 241-260.
657 3 Mcnamara K, Tofail SAM, Mcnamara K, Tofail SAM. Advances in Physics : X
658 Nanoparticles in biomedical applications. *Adv Phys X* 2017; 2: 1–35.
659 4 Severino P, Szymanski M, Favaro M, Azzoni AR, Chaud M V., Santana MHA,
660 Silva AM, Souto EB. Development and characterization of a cationic lipid
661 nanocarrier as non-viral vector for gene therapy. *Eur J Pharm Sci* 2015; 66: 78–
662 82.
663 5 Marangoni VS, Bernardi JC, Reis IB, Favaro WJ, Zucolotto V. Photothermia and
664 Activated Drug Release of Natural Cell Membrane Coated Plasmonic Gold
665 Nanorods and β - Lapachone. *Appl. Bio Mater* 2019; 2, 728-736.
666 6 Fang RH, Hu CJ, Luk BT, Gao W, Copp JA, Tai Y *et al.* Cancer Cell Membrane-

667 Coated Nanoparticles for Anticancer Vaccination and Drug Delivery. *Nano Lett*
668 2014; 14: 2181−2188
669 7 Govender R, Phulukdaree A, Gengan RM, Anand K, Chuturgoon AA. Silver
670 nanoparticles of Albizia adianthifolia : the induction of apoptosis in human lung
671 carcinoma cell line. *J. Nanobiotechnology* 2013; 11: 1–9.
672 8 Guo D, Zhu L, Huang Z, Zhou H, Ge Y, Ma W, Wu J, Zhang X, Zhou X, Zhang
673 Y, Zhao Y, Gu N. Anti-leukemia activity of PVP-coated silver nanoparticles via
674 generation of reactive oxygen species and release of silver ions. *Biomaterials* 2013;
675 34: 7884–7894.
676 9 Miethling-Graff R, Rumpker R, Richter M, Verano-Braga T, Kjeldsen F, Brewer
677 J, Hoyland J, Rubahn HG, Erdmann H. Exposure to silver nanoparticles induces
678 size- and dose-dependent oxidative stress and cytotoxicity in human colon
679 carcinoma cells. *Toxicol In Vitro* 2014; 28: 1280–9.
680 10 Lim HK, Gurung RL, Hande MP. DNA-dependent protein kinase modulates the
681 anti-cancer properties of silver nanoparticles in human cancer cells. *Mutat Res -*
682 *Genet Toxicol Environ Mutagen* 2017; 824: 32-41
683 11 Park S, Lee MJ, Lee SJ, Yun SJ, Jang J-Y, Kang H Kim K, Choi I, Park S. Silver
684 nanoparticles affect glucose metabolism in hepatoma cells through production of
685 reactive oxygen species. *Int J Nanomedicine* 2015; 11: 55-68.
686 12 Miranda RR, Gorshkov V, Korzeniowska B, Kempf SJ, Neto FF, Kjeldsen F. Co-
687 exposure to silver nanoparticles and cadmium induce metabolic adaptation in
688 HepG2 cells. *Nanotoxicology* 2018; 12: 781–795.
689 13 Miranda RR, Bezerra AG, Ribeiro CAO, Randi MAF, Voigt CL, Skytte L,
690 Rasmussen KL, Kjeldsen F, Filipak Neto F. Toxicological interactions of silver
691 nanoparticles and non-essential metals in human hepatocarcinoma cell line.

Toxicol Vitr 2017; 40: 134–143.

14 Kovács D, Szoke K, Igaz N, Spengler G, Molnár J, Tóth T, Madarász D, Rázga Z, Kónya Z, Boros IM, Kiricsi M. Silver nanoparticles modulate ABC transporter activity and enhance chemotherapy in multidrug resistant cancer. *Nanomedicine Nanotechnology, Biol Med* 2016; 12 601–610

15 Ignat E V, Volkov NM, Snetov VN, Stogov AY. Effect of Silver Oxide Nanoparticles on Tumor Growth in Vivo. 2008; 421: 274–276.

16 Sriram MI, Barath S, Kanth M, Kalishwaralal K, Gurunathan S. Antitumor activity of silver nanoparticles in Dalton ' s lymphoma ascites tumor model. *Int J Nanomedicine* 2010; 5: 753–762.

17 Swanner J, Mims J, Carroll DL, Akman SA, Furdui CM, Torti S V, Singh RN. Differential cytotoxic and radiosensitizing effects of silver nanoparticles on triple-negative breast cancer and non-triple-negative breast cells. *Int J Nanomedicine* 2015; 10: 3937–3953.

18 Schwämmle V, León IR, Jensen ON. Assessment and improvement of statistical tools for comparative proteomics analysis of sparse data sets with few experimental replicates. *J Proteome Res* 2013; 12: 3874–3883.

19 Doncheva NT, Morris J, Gorodkin J, Jensen LJ. Cytoscape stringApp : Network analysis and visualization of proteomics data. *J. Proteome Res* 2019; 18: 623-632

20 Elbaz NM, Ziko L, Siam R, Mamdouh W. Core-Shell Silver / Polymeric Nanoparticles-Based Combinatorial Therapy against Breast Cancer. *Nat Publ Gr* 2016; 6: 1–9.

21 Yang L, Gao Y, Liu J, Zhang Y, Ren C, Wang J, Wang Z, Liu J, Chu L, Wang W, Huang F. Silver-coated nanoparticles combined with doxorubicin for enhanced anticancer therapy. *J Biomed Nanotechnol* 2018; 14: 312–320.

717 22 Zhang XF, Gurunathan S. Combination of salinomycin and silver nanoparticles
718 enhances apoptosis and autophagy in human ovarian cancer cells : an effective
719 anticancer therapy. *Int J Nanomedicin* 2016; 11: 3655–3675.
720 23 Yuan YG, Peng Q, Gurunathan S. Silver nanoparticles enhance the apoptotic
721 potential of gemcitabine in human ovarian cancer cells : combination therapy for
722 effective cancer treatment. *Int J Nanomedicin* 2017; 12: 6487–6502.
723 24 Trachootham D, Alexandre J, Huang P. Targeting cancer cells by ROS-mediated
724 mechanisms: a radical therapeutic approach? *Nat Rev Drug Discov* 2009; 8: 579–
725 591.
726 25 Li Y, Guo M, Lin Z, Zhao M, Xiao M, Wang C Xu T, chen T, Zhu B.
727 Polyethylenimine-functionalized silver nanoparticle-based co-delivery of
728 paclitaxel to induce HepG2 cell apoptosis. *Int J Nanomedicine* 2016; 11: 6693–
729 6702.
730 26 Luqmani YA. Mechanisms of drug resistance in cancer chemotherapy. *Med Princ*
731 *Pract* 2005; 14: 35–48.
732 27 Rodríguez-Enríquez S, Juárez O, Rodríguez-Zavala JS, Moreno-Sánchez R.
733 Multisite control of the Crabtree effect in ascites hepatoma cells. *Eur J Biochem*
734 2001; 268: 2512–2519.
735 28 Liberti M V., Locasale JW. The Warburg Effect: How Does it Benefit Cancer
736 Cells? *Trends Biochem Sci* 2016; 41: 211–218.
737 29 Mauro C, Leow SC, Anso E, Rocha S, Thotakura AK, Tornatore L, Moretti M,
738 Smaele E, Beg AA, Tergaonkar V, Chandel NS, Franzoso G. NF- κ B controls
739 energy homeostasis and metabolic adaptation by upregulating mitochondrial
740 respiration. *Nat Cell Biol* 2011; 13: 1272–1279.
741 30 DeBerardinis RJ, Lum JJ, Hatzivassiliou G, Thompson CB. The Biology of

Cancer: Metabolic Reprogramming Fuels Cell Growth and Proliferation. *Cell Metab* 2008; 7: 11–20.

31 Carracedo A, Cantley LC, Pandolfi PP. Cancer metabolism: fatty acid oxidation in the limelight. *Nat Rev Cancer* 2013; 13: 227–32.

32 Chen JQ, Russo J. Dysregulation of glucose transport, glycolysis, TCA cycle and glutaminolysis by oncogenes and tumor suppressors in cancer cells. *Biochim Biophys Acta - Rev Cancer* 2012; 1826: 370–384.

33 Takanaga H, Chaudhuri B, Frommer WB. GLUT1 and GLUT9 as major contributors to glucose influx in HepG2 cells identified by a high sensitivity intramolecular FRET glucose sensor. *Biochim Biophys Acta - Biomembr* 2008; 1778: 1091–1099.

34 Staels B, Bosscher K De. Molecular Actions of PPAR a in Lipid Metabolism and In fl ammation. *Endocr Rev* 2018; 39(5): 760–802.

35 Mikłosz A. The Implication of PGC-1 α on Fatty Acid Transport across Plasma and Mitochondrial Membranes in the Insulin Sensitive Tissues. *Front. Physiol* 2017; 8: 1–16.

36 Guo D, Bell EH, Mischel P, Chakravartia A. Targeting SREBP-1-driven lipid metabolism to treat cancer. *Curr Pharm Des* 2014; 20: 2619–2626.

37 Gosmain Y, Dif N, Berbe V, Loizon E, Rieusset J, Vidal H *et al.* Regulation of SREBP-1 expression and transcriptional action on HKII and FAS genes during fasting and refeeding in rat tissues. *J lipid res* 2005; 46: 697–705.

38 Iizuka K. Biochimica et Biophysica Acta The transcription factor carbohydrate-response element-binding protein (ChREBP): A possible link between metabolic disease and cancer. *BBA - Mol Basis Dis* 2017; 1863: 474–485.

39 Lee IH. Mechanisms and disease implications of sirtuin-mediated autophagic

767 regulation. *Exp Mol Med* 2019; 51: 1–11.

768 40 Finkel MT, Deng CX, Mostoslavsky R. Recent progress in the biology and
769 physiology of sirtuin. *Nature* 2009; 460: 587–591.

770 41 Chang HC, Guarente L. SIRT1 and other sirtuins in metabolism. *Trends*
771 *Endocrinol Metab* 2014; 25: 138–145.

772 42 Silver DP, Livingston DM. Mechanisms of BRCA1 tumor suppression. *Cancer*
773 *Discov* 2012; 2: 679–684.

774 43 Yarden RI, Pardo-Reoyo S, Sgagias M, Cowan KH, Brody LC. BRCA1 regulates
775 the G2/M checkpoint by activating Chk1 kinase upon DNA damage. *Nat Genet*
776 2002; 30: 285–289.

777 44 Blair LP, Cao J, Zou MR, Sayegh J, Yan Q. Epigenetic regulation by lysine
778 demethylase 5 (KDM5) enzymes in cancer. *Cancers (Basel)* 2011; 3: 1383–1404.

779 45 Liang X, Zeng J, Wang L, Shen L, Ma X, Li S, Ma X, Li S, Wu Y, Ma L, Ci X,
780 Guo Q, Jia M, Shen H, Sun Y, Liu Z, Liu S, Li W, Yu H, Chen C, Jia J. Histone
781 demethylase RBP2 promotes malignant progression of gastric cancer through
782 TGF-β1-(p-Smad3)-RBP2-E-cadherin-Smad3 feedback circuit. *Oncotarget* 2015;
783 6: 17661–17674.

784 46 Maggi EC, Trillo-Tinoco J, Struckhoff AP, Vijayaraghavan J, Del Valle L,
785 Crabtree JS. Retinoblastoma-binding protein 2 (RBP2) is frequently expressed in
786 neuroendocrine tumors and promotes the neoplastic phenotype. *Oncogenesis* 2016;
787 5: e257.

788 47 Dyson NJ. RB1: A prototype tumor suppressor and an enigma. *Genes Dev* 2016;
789 30: 1492–1502.

790 48 Holmström KM, Finkel T. Cellular mechanisms and physiological consequences
791 of redox-dependent signalling. *Nat Rev Mol Cell Biol* 2014; 15: 411–21.

792 49 Motohashi H, Yamamoto M. Nrf2 – Keap1 defines a physiologically important
793 stress response mechanism. *Trends. Mol. Med* 2004; 11: 549-557.
794 50 Vriend J, Reiter RJ. The Keap1-Nrf2-antioxidant response element pathway: A
795 review of its regulation by melatonin and the proteasome. *Mol. Cell. Endocrinol*
796 2015; 401: 213–220.
797
798